Electrochemical Synthesis of Gold Nanocrystals and Their 1D and 2D Organization

Shaoxin Huang,[†,‡] Houyi Ma,[*,†,‡] Xiaokai Zhang,[§] Feifei Yong,[‡] Xingli Feng,[‡] Wei Pan,[‡] Xuning Wang,[‡] You Wang,[||] and Shenhao Chen[‡,⊥]

Key Laboratory for Colloid and Interface Chemistry of State Education Ministry, Shandong University, Jinan 250100, China, Department of Chemistry, Shandong University, Jinan 250100, China, Testing Center, Shandong Normal University, Jinan 250014, China, Department of Materials Science, School of Materials Science and Engineering, Harbin Institute of Technology, Harbin 150001, China, and State Key Laboratory for Corrosion and Protection of Metals, Shenyang 110015, China

Received: May 30, 2005; In Final Form: July 31, 2005

Size-controlled gold nanocrystals were conveniently synthesized through direct electroreduction of bulk $AuCl_4^-$ ions in the presence of poly(*N*-vinylpyrrolidone) (PVP). PVP greatly enhanced the gold particle formation process and also significantly retarded the gold electrodeposition process, allowing the electrochemical synthesis of gold nanocrystals to be carried out in the form of simple electroreduction. This novel electrochemical method may be extended to synthesis of other noble metal nanoparticles with controllable size on a large scale. The PVPK90-protected gold nanocrystals spontaneously self-assembled into nearly ordered 2D close-packed arrays and interesting 1D nanostructures. The aggregation of unstable PVPK17-protected gold nanocrystals resulted in the formation of ultrathin single-crystalline films. PVP plays multifunctional roles in controlling the size and shape of gold nanocrystals and in inducing individual gold nanocrystals to construct 1D nanostructures. The nanoparticle self-assembling technique based on PVP offers a simple, but effective, path to organize individual gold nanoparticles into various 1D and 2D nanostructured materials.

1. Introduction

Gold and other noble metal nanocrystals have received increasing interest in various fields of chemistry due to their important roles in different branches of science,[1] such as chemical catalysis,[2] nanomedicines,[3] and nanoelectronics.[4] The intrinsic properties of a metal nanoparticle strongly depend on its size, shape, composition, crystallinity, and structure.[5] Precise control of size, shape, structure, and morphology of nanoparticles has been one of the most attractive goals for the synthetic chemists in this field.[6−8] On the other hand, the assembly of nanoparticles is a key step for their application as nanodevices,[9,10] which is as important as the preparation of nanosized particles, even more important in the aspect of fabrication of nanometer-scale functional materials. Consequently, the exploration concerning synthesis of size- and shape-controlled nanoparticles and assembly of nanoparticles into desired nanostructures is becoming a challenging research area in current nanotechnology and nanomaterials manufacturing.[5,6,11,12]

Some advantages of electrochemical methods over chemical ones in synthesis of metal nanostructures are the high purity of products and good control of size, shape, and morphology of the nanostructured materials.[6,8] Well-defined nanowire and nanorods of pure metals or metal compounds have been prepared through electrodeposition in a membrane template[13] or at step edges on graphite.[14] However, the use of hard templates may complicate the synthetic procedure and limit the synthesis of nanostructured materials in large quantities.[15] We are therefore more interested in the size-selective and shape-controlled electrochemical synthetic methods based on the use of multifunctional ligands, polymers, and surfactants as the stabilizers and shape-controllers.[6,8a,16,17] This type of electrochemical method was first proposed by Reetz and Helbig in 1994;[8a] then it was further developed to prepare silver nanoparticles either in acetonitrile solution by Rodriguez-Sanchez et al.[16a] or in aqueous solution by us,[6] and to prepare gold nanorods in aqueous solution by Mohamed et al.[17a] and Chang et al.[17b,c] A large number of nanostructured metallic materials can be synthesized through a simple electroreduction of metal ions by using this method.

In this paper, we describe a simple and effective method to electrochemically synthesize size- and shape-controlled gold nanocrystals under the protection of poly(*N*-vinylpyrrolidone) (PVP). The most distinguished features of the present method include ease of operation, high yield, uniformity of nanocrystals, absence of undesired byproducts, and large-scale synthesis of noble metal nanocrystals. More significantly, the as-synthesized gold nanocrystals are easily used as "building blocks" to construct one-dimensional (1D) nanostructures, such as nanowires and nanorings, and two-dimensional (2D) ordered close-packed nanoaggregates, without requiring complicated assembling procedures or laborious processes. These novel nanostructures are promising for construction of future nanodevices and nanocircuits.

PVP has been extensively applied in the chemical, photochemical, and electrochemical synthesis of gold, silver, and other noble metal nanoparticles.[5,18−23] PVP is a homopolymer with a long and soft polyvinyl chain, whose monomer has a hydrophilic cyclic amide group. The nitrogen and oxygen atoms of this polar

* Corresponding author. Fax: +86-531-88564464. E-mail: hyma@sdu.edu.cn.
† Key Laboratory for Colloid and Interface Chemistry of State Education Ministry, Shandong University.
‡ Department of Chemistry, Shandong University.
§ Testing Center, Shandong Normal University.
|| Harbin Institute of Technology.
⊥ State Key Laboratory for Corrosion and Protection of Metals.

10.1021/jp052863q CCC: $30.25
Published on Web 10/04/2005

group have a strong affinity for gold, silver, platinum, and palladium ions and their metallic clusters.[23b] Therefore, PVP is generally considered to act as both the coordinating agent for the metallic ions and the stabilizing agent for the formed metallic nanoparticles during synthesis of nanosized noble metal particles.[6,23] However, the actions of PVP are not just confined to the above-mentioned two functions and are probably multifunctional. For example, Sun and Xia[15] demonstrated that PVP would function as a capping agent in the preparation of bicrystalline silver nanowires. The present study shows that PVP still plays multiples roles in controlling the size of nanocrystals, in enhancing or limiting the growth rate of certain gold crystal planes, as well as in inducing individual gold nanocrystals to form a variety of intriguing 1D nanostructures.

2. Experimental Section

2.1. Voltammetric Measurements. Pt and Au wires with 0.8-mm diameter (Aldrich, 99.9%) were employed to prepare the working electrodes. A wire specimen was embedded in the epoxy resin mold, and only its cross section was allowed to contact the electrolytes. Before each experiment, the Pt or Au electrode was ground with SiC abrasive papers of decreasing particle size to #2000 finish, then rinsed with triple distilled water and alcohol.

The cyclic voltammetric measurements were performed with a Zahner IM6 electrochemical workstation in a conventional three-electrode cell at room temperature (~22 °C). A 1.0-cm × 2.0-cm platinum and a saturated calomel electrode (SCE) were used as the counter electrode and the reference electrode, respectively. The reference electrode was led to the surface of the working electrode through a Luggin capillary. The solutions were deoxygenated by bubbling of high-purity N_2 in the solutions before measurements. The potentials were measured against the SCE at first, then converted into the values with reference to the standard hydrogen electrode (SHE).

Cyclic voltammograms (CVs) for the Pt and Au electrodes were acquired through a linear potential scan from the open-circuit potential (E_{ocp}) to the negative potential vertex, then to the positive potential vertex, and finally backward to the initial potential at a designated scan rate.

2.2. Electrochemical Synthesis of Gold Nanocrystals. The electrochemical synthesis of gold nanocrystals was carried out in a two-electrode cell. A rotating platinum electrode made from a 2.0-mm diameter platinum rod (Aldrich, 99.9%) was used as the cathode, and a 1.0 cm × 2.0 cm platinum sheet was used as the anode. The rotation speed of the cathode was controlled at 1000 rpm unless otherwise indicated.

All chemicals were of analytical grade and were used without further purification. The electrolytic solutions for the synthesis of gold nanocrystals consisted of 0.1 mol dm^{-3} KNO_3, 5.0 × 10^{-4} mol dm^{-3} $HAuCl_4$, and poly(*N*-vinylpyrrolidone) (PVP) (BASF). Three kinds of PVP reagents with the same structure but different chain length, K90 (average molecular weight ($\bar{M}_w$): 360000), K30 (M_w: 40000), and K17 ($\bar{M}_w$: 10000), served, respectively, as the stabilizers and size (or shape) controllers for gold nanocrystals in the process of electrochemical synthesis. The electrolysis was conducted in the galvanostatic manner at room temperature (~22°). The current chosen was 100 mA, and the electrolysis time was 5 min. The gold colloids were placed for 48 h before TEM measurements.

2.3. Characterization of Gold Nanocrystals. The samples for TEM measurements were prepared by putting a drop of the colloidal gold dispersion onto a standard microscope grid coated with a Formvar film, followed by natural evaporation of the solvent. The TEM photographs were taken with a Hitachi H-800 transmission electron microscope operated at a 200 kV accelerating voltage. The crystallinity of the PVP-protected gold nonocrystals was characterized by high-resolution electron transmission microscopy (HRTEM) and an electron diffraction (ED) pattern on a Philips Tecnai20U-TWIN operated at 200 kV. EDS analysis data for individual gold nanoparticles were recorded by an EDAX9100 installed at the Philips Tecnai20U-TWIN. The UV−vis absorption spectra were measured with a Hitachi U-4100 UV−vis spectrophotometer using a 1-cm path-length cell.

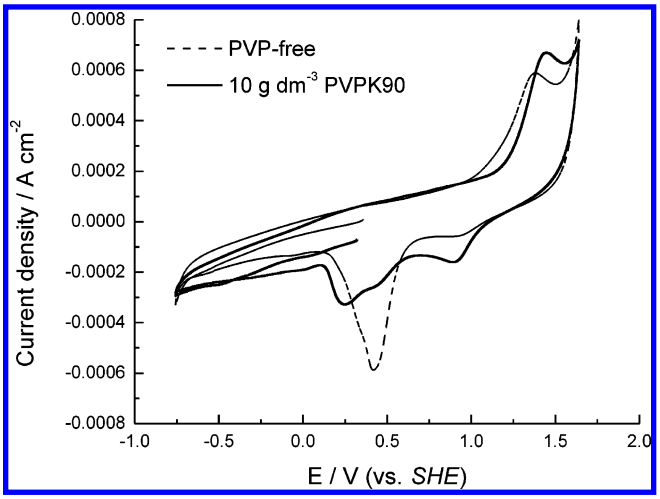

Figure 1. Cyclic voltammograms for Au/0.1 mol dm^{-3} KNO_3 (pH 7) in the absence (dash line) and in the presence (solid line) of 10 g dm^{-3} PVPK90, scan rate 50 mV s^{-1}. The open-circuit potentials (E_{ocp}) of the Au electrode in PVP-free and PVP-containing solutions are 0.36 and 0.32 V, respectively.

3. Results and Discussion

3.1. Cyclic Voltammograms (CVs). Figure 1 shows cyclic voltammograms (CVs) at 50 mV s^{-1} for an Au electrode in 0.1 mol dm^{-3} KNO_3 solutions with and without PVP, respectively. In the absence of PVP, the CVs of the Au electrode did not exhibit any reduction peak in the first negative-going scan from the open-circuit potential (E_{ocp} = 0.36 V) to the negative potential maximum, but gave an oxidation peak at 1.37 V in the positive-going scan and a reduction peak at 0.42 V in the second negative-going scan. The oxidation peak originates from the formation of gold oxide on the electrode surface, and the reduction peak is attributed to subsequent reduction of the oxide during the negative potential sweep.[24] However, the presence of PVP led to the great variation of voltammetric behavior of the Au electrode. It is observed from the CVs of the Au electrode in the PVP-containing solution that the previous reduction peak at 0.42 V was suppressed to a considerable degree and the peak maximum was shifted about 0.17 V in the negative potential direction; besides, a new reduction peak appeared at more positive potential (about 0.90 V). Seeing that N and O atoms of the cyclic amide group in PVPs have a strong affinity for transition metal ions and their metallic clusters,[23b] the coordination of the N and O atoms of PVP with the gold ions produced in the electrochemical oxidation makes the reduction of gold oxide proceed in the form of the stepwise electrochemical reduction.

Figure 2a shows CVs of a Pt electrode in the PVP-free and PVP-containing electrolytic solutions of KNO_3 (0.1 mol dm^{-3}) and $HAuCl_4$ (5.0 × 10^{-4} mol dm^{-3}) at 50 mV s^{-1}, respectively. The current−potential profile describing redox processes of the

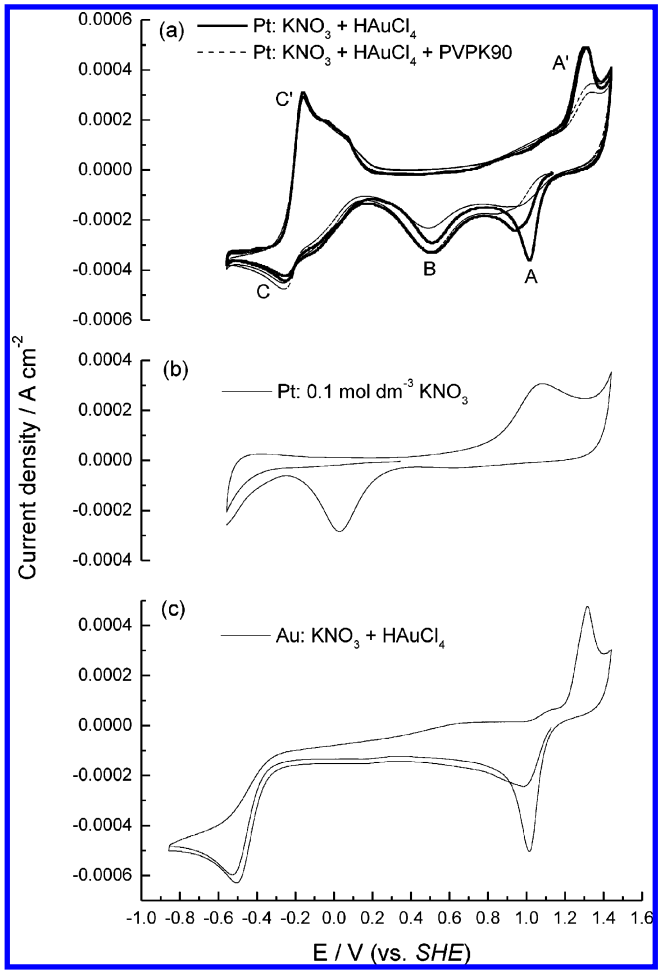

Figure 2. (a) Cyclic voltammograms (CVs) for the redox reactions of gold species at a Pt electrode in 0.1 mol dm^{-3} KNO_3 + 5 × 10^{-4} mol dm^{-3} $HAuCl_4$ solution (pH 3.13) and in 0.1 mol dm^{-3} KNO_3 + 5 × 10^{-4} mol dm^{-3} $HAuCl_4$ + 10 g dm^{-3} PVPK90 solution (pH 3.23), scan rate 50 mV s^{-1}. The open-circuit potentials (E_{ocp}) of the Pt electrode in the absence and presence of PVP are 1.14 and 1.13 V, respectively. (b) CVs at 50 mV s^{-1} for a Pt electrode in 0.1 mol dm^{-3} KNO_3 solution (pH 7). E_{ocp} = 0.34 V. (c) CVs of an Au electrode in 0.1 mol dm^{-3} KNO_3 + 5 × 10^{-4} mol dm^{-3} $HAuCl_4$ solution (pH 3.13) at 50 mV s^{-1}. E_{ocp} = 1.13 V.

gold species is complicated, because the Au metal center possesses a valence state of 3. The CVs displayed three reduction peaks (A, B, and C) and two oxidation peaks (A′ and C′), irrespective of the presence of PVP. We have done two contrast experiments to determine the origin of the above-mentioned current peaks. One is the measurement of the CVs for the Pt electrode in 0.1 mol dm^{-3} KNO_3 solution (Figure 2b). The CVs shown in Figure 2b presented an oxidation peak at 1.07 V and a reduction peak at 0.03 V, which arise, respectively, from the formation of platinum oxide on the surface and the subsequent reduction. The other is to measure the CVs of the Au electrode in the mixed solution of 0.1 mol dm^{-3} KNO_3 and 5.0 × 10^{-4} mol dm^{-3} $HAuCl_4$ (Figure 2c). The CVs obtained are obviously different from those of the Pt electrode in the same solution, which show a pair of quasi-reversible redox peaks at potentials over 1.0 V and a reduction peak initiating at −0.30 V, as shown by Figure 2c.

By comparing the CVs of the Pt and Au electrodes in different solutions, the origin of the current peaks in the CVs of the Pt electrode in the KNO_3 solutions containing $HAuCl_4$ is interpreted as follows: peaks A are associated with the simultaneous reduction of both Au^{III} to Au^{I} and Au^{III} to Au^0, and peak A′ is the quasi-reversible oxidation peak of reduction peak A. Theoretically, the standard potential (0.926 V)[25] for the reaction $AuCl_4^- + 2e^- = AuCl_2^- + 2Cl^-$ is close to that (1.02 V)[25] for the reaction $AuCl_4^- + 3e^- = Au + 4Cl^-$. As a result, the electrochemical reduction of $AuCl_4^-$ at about 1.0 V (peak A) probably involves two reduction processes of both $AuCl_4^-$ to $AuCl_2^-$ and $AuCl_4^-$ to Au^0 species at the same time. Peak B should be due to the reduction of Au^I−PVP complexes on the basis of the voltammetric properties of the Au electrode in KNO_3 solutions with and without PVP. Peak C is ascribed to the hydrogen adsorption on the platinum surface and the subsequent evolution reaction; conversely, peak C′ is caused by the desorption of hydrogen from the platinum surface. In contrast, Figure 2c indicates that the hydrogen evolution reaction took place at a more negative potential on the gold surface than on the platinum surface because of the higher overpotential potential for the hydrogen evolution on the gold surface.[26]

The voltammetric behavior of $HAuCl_4$ at the Pt electrode greatly changed after PVPK90 was added into a $HAuCl_4$ + KNO_3 mixed solution. By comparing the CVs of the Pt electrode in the presence and absence of PVP (see Figure 2a), it is found that PVP strongly inhibited both peaks A and A′. The Au^0 products formed through the electroreduction were divided into two parts:[6,16,21] one portion of the products consisted of the gold depositions on the cathode surface, which were subsequently oxidized in the process of anodic sweep, resulting in the oxidation peak A′; another portion of products consisted of gold particles, which entered the bulk phase of the electrolyte without being oxidized in the subsequent anodic sweep. The negative potential shift of peak A in the presence of PVP implies that the gold electrodeposition rate was lowered by PVP. A decrease in current of oxidation peak A′ in the PVP-containing solution further indicates that the electrodeposition process of Au^{III} (or Au^I) species was effectively suppressed and large amounts of $AuCl_4^-$ ions were directly reduced to gold nanoparticles in the negative potential sweep. The hydrogen evolution reaction also benefits the formation of gold nanoparticles since the fresh, active hydrogen produced on the platinum surface is able to reduce the bulk $AuCl_4^-$ ions, forming gold particles.

The potential scan rate strongly affected the size and height of the current peaks, but it had little influence on their positions. The faster the scan rate, the larger the peak current. The decrease in the $HAuCl_4$ concentration markedly lowered the oxidation and reduction peaks of Au species and also changed the potential for the hydrogen evolution reaction.

It is of interest that the color of the PVP-containing electrolytes changed from orange to claret-red when the platinum electrode was consecutively scanned for 50 cycles by a triangular potential cycling between −0.56 and 1.44 V. In contrast, no obvious color change was observed for the PVP-free electrolyte during the same potential cycling. The change in the color of PVP-containing electrolytes attracted our attention to the formation of gold nanoparticles. UV−vis spectrophotometry was used to further determine whether or not the gold nanoparticles formed.

Figure 3 shows a set of UV−vis absorption spectra for the KNO_3 + $HAuCl_4$ + PVP electrolytes after being pretreated by the consecutive potential cycling in the different potential region. Evidently, the spectroscopic behavior of the absorption spectra is dependent on the potential scan range to be selected, especially the negative and positive potential vertexes. Among the four UV−vis spectra in Figure 3, curves 2 and 4 displayed the obvious absorbance bands corresponding to the characteristic plasmon band of spherical gold nanoparticles, whereas curves

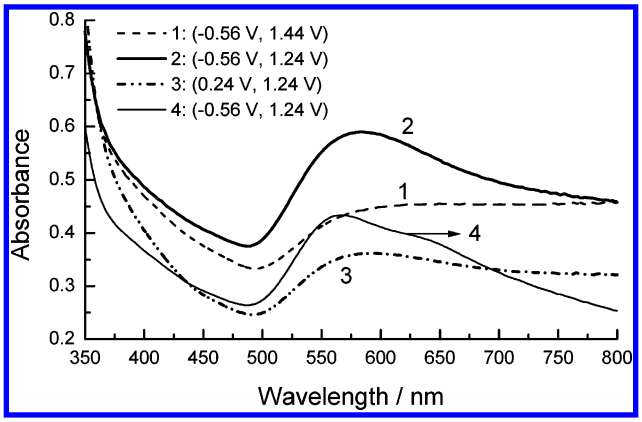

Figure 3. UV-vis absorption spectra obtained after a 50-cycle potential cycling at 50 mV s^{-1} in the PVP-containing electrolytes in the designated potential range marked in the figure. Curves 1, 2, 3: in 0.1 mol dm^{-3} KNO_3 + 5 × 10^{-4} mol dm^{-3} $HAuCl_4$ + 20 g dm^{-3} PVP K90; Curve 4: in 0.1 mol dm^{-3} KNO_3 + 5 × 10^{-4} mol dm^{-3} $HAuCl_4$ + 20 g dm^{-3} PVP K30.

1 and 3 did not give the whole absorbance bands although they tended to form the absorbance band in the characteristic absorbance region of gold nanoparticles. On the basis of Figure 3, it is concluded that the potential region between −0.56 and 1.24 V is an ideal potential region which is applicable for the electrochemical synthesis of gold nanoparticles by a consecutive potential cycling. It is unfavorable for the electrochemical synthesis of gold nanoparticles to choose a positive potential over 1.24 V as the positive potential maximum, because the gold adatoms or gold nonoclusters produced in the negative potential sweep will be oxidized again at very high anodic potentials. This conclusion is supported by the cyclic voltammetric results shown in Figure 2a. It is seen from Figure 2a that two reduction peaks (A and B) caused by the stepwise reduction of Au^{III} ions and another reduction peak (C) originating from the hydrogen evolution are all in this potential region; however, the oxidation peak (A′) is not in the potential range.

The electrochemical reduction of metal ions usually involves two competing cathode processes:[6,16,21] one corresponds to the formation of metal particles and the other corresponds to the electrodeposition onto the cathode. The former process must be minimized and the latter one must be promoted in order to realize electrochemical synthesis of metal nanoparticles. In this sense, the choice of an ideal stabilizer is one of technological keys to electrochemical synthesis of metallic nanoparticles. Compared with quaternary ammonium salts widely used for the stabilization of transition metal nanoparticles,[8a,8d,16,17] PVP is a polymeric ligand which not only acts as a good coordination agent for many transition metal ions but also has a very strong affinity toward their metallic clusters,[23b] especially for gold, silver, and platinum nanoclusters.[6,21,19b] The use of PVP greatly inhibited the electroreduction trend of Au^{III} ions at the cathode, making the particle-formation process dominate significantly over the electrodeposition process during electroreduction of Au^{III} ions. This conclusion has been supported by the electrochemical synthesis of gold nanoparticles through a potential cycling in the designated potential range.

Considering that the hydrogen evolution is favorable toward formation of metal particles,[16a] electrochemical synthesis of gold nanoparticles is expected to take place in manner of simple electroreduction when a large negative current is applied to the cathode.

3.2. TEM and HRTEM Characterization of Gold Nanocrystals. The electrolyte for electrochemical synthesis of monodispersed gold nanocrystals was composed of $HAuCl_4$ (5.0 × 10^{-4} mol dm^{-3}), KNO_3 (0.1 mol dm^{-3}), and PVPK90 (30 g dm^{-3}, $\bar{M}_w$: 360000). Different from previous studies,[8a,8c,16,17] the bulk metallic ions were not converted from the sacrificial anode but instead came directly from the electrolyte, which is favorable for large-scale synthesis of gold nanocrystals. The use of KNO_3 as the main supporting electrolyte avoided the variation of the solution resistance caused by the gradual depletion of $AuCl_4^-$ ions and maintained the relative stability of the current density. This is of great importance to the size-controlled electrochemical synthesis of nanoparticles. The application of a rotating platinum cathode greatly accelerated the transfer of the gold nanoparticles synthesized electrochemically from the cathodic vicinity to the bulk solution, effectively avoiding occurrence of flocculates in the vicinity of the cathode and ensuring the monodispersity of the particles.

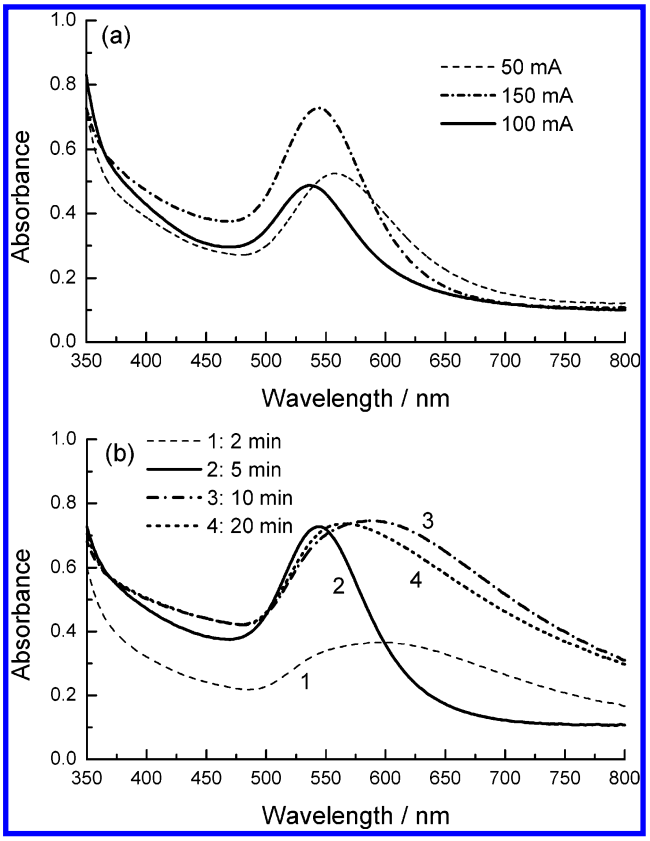

Figure 4. UV-vis absorption spectra for the gold colloidal solutions obtained at different current (a) or in the case of different electrolysis time (b) by using PVPK90 as the stabilizer.

Figure 4a depicts a set of absorbance spectra with good symmetry for gold nanoparticles synthesized by applying different current to the two-electrode cell system. Theoretically, a decrease in particle size can induce a decrease in the plasmon band intensity.[21,27] The higher the absorbance of the gold nanoparticles, the larger their size is. Accordingly, the applied current of 100 mA was suitable for synthesis of gold particles with small size. Figure 4b shows the evolution of UV−vis absorbance spectra for the gold colloidal solutions with the electrolysis time. Among four spectra, curve 2 exhibited a relatively symmetrical absorbance band around 540 nm, characteristic of nanosized gold particles. The good symmetry for the characteristic absorption band of nanoparticles indicates that the gold nanoparticles synthesized in the case of the 5-min electrolysis time had a narrow particle size distribution.[21] On the basis of the UV−vis spectroscopic studies, the applied current and the electrolysis time for electrochemical synthesis

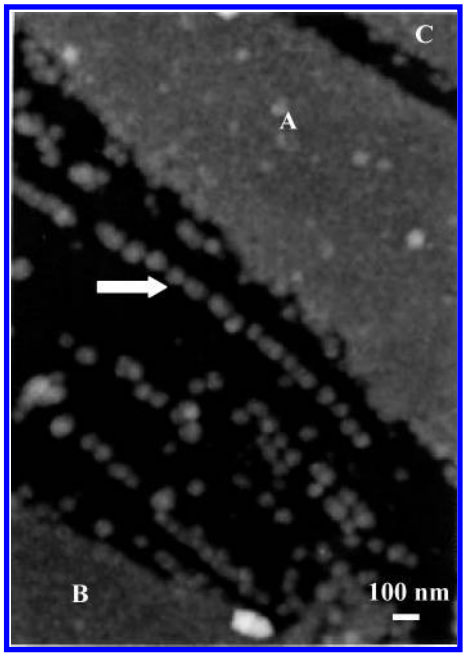

Figure 5. A typical low-magnification TEM image for gold nanoparticles electrochemically synthesized in an aqueous solution of 5.0×10^{-4} mol dm^{-3} $HAuCl_4$ + 0.1 mol dm^{-3} KNO_3 + 30 g dm^{-3} PVPK90. An arrow points to the wire-shaped nanoparticle aggregates.

of monodispersed gold nanoparticles were determined to be 100 mA and 5 min, respectively. The effect of the rotating speed of the working electrode on the particle size has been studied previously.[21] The rotating speed of 1000 rpm is applicable for acquiring monodispersed metallic nanoparticles with small size.

Figure 5 shows a representative large-scale TEM image of gold nanoparticles synthesized electrochemically. A large amount of particles constituted close-packed aggregates in regions A, B, and C. In addition, there existed the wirelike nanoparticle assemblies and individual particles between regions A and B. Especially, close to 20 gold nanoparticles linked together, making up a discontinuous wire-shaped nanostructure of about 1.32 μm in length. A careful inspection shows that at some points there is adhesion of neighboring nanoparticles. A similar phenomena also happen in the ring-shaped nanoparticle assemblies (see section 3.4). Fusion between nanoparticles will take place only when suitable crystallographic facets are facing each other.[28] Very obviously, gold nanoparticles did not randomly distribute on the surface of a TEM grid but spontaneously self-assembled into the ordered 1D nanostructures and the compact 2D aggregates on the grid surface.

A high-magnification TEM micrograph was obtained by enlarging a selected part of region A in Figure 5, as shown by Figure 6a. This image shows more clearly that the gold particles were not only approximately uniform in size and shape, but also two-dimensionally ordered to a certain degree. Moreover, some particles with almost identical size adopted a hexagonal close-packing. The particle size distribution is shown as a histogram in Figure 6b. A Gaussian fit illustrates that these particles had a mean particle diameter of 42.4 nm, with a standard deviation of 3.87 nm.

Metal nanoparticles need to meet the following three conditions in order to self-assemble into the periodic arrays: (i) relatively high particle concentration, (ii) good uniformity in both size and shape, (iii) sufficient stability provided by adsorbed capping ligands.[10] Although the close-packed arrangements of the nanoparticles in Figure 6a seemed not very perfect, it should

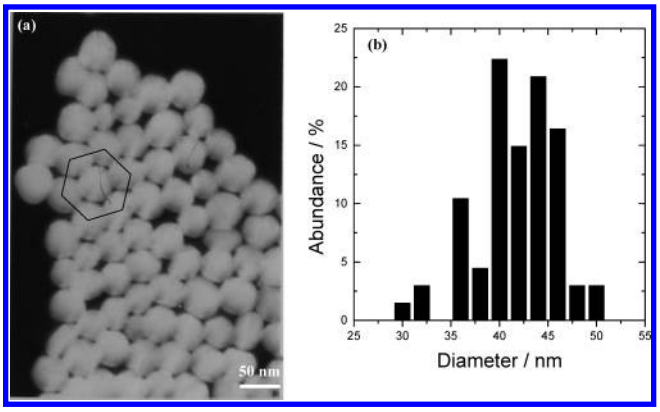

Figure 6. (a) A high-magnification TEM image of gold nanoparticles electrochemically synthesized in an aqueous solution of 5.0×10^{-4} mol dm^{-3} $HAuCl_4$ + 0.1 mol dm^{-3} KNO_3 + 30 g dm^{-3} PVPK90. A hexagon was superimposed on the image in order to depict the close-packed manner of gold nanoparticles with uniform size and shape. (b) Particle size distribution of gold nanoparticles obtained by measuring the diameter of gold particles in Figure 6a.

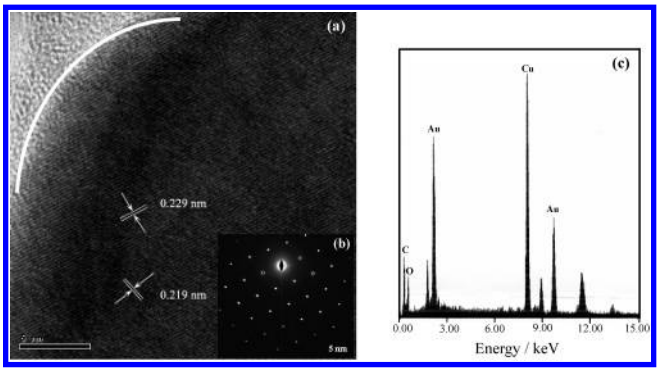

Figure 7. (a) High-resolution transmission electron microscopic (HRTEM) image of a randomly selected gold particle. A white curve marks the boundary between the gold particle and the HRTEM grid. The top left corner shows the image of the HRTEM grid, and the rest displays the two-dimensional lattice image of an individual gold particle. The scale bar is 5 nm. (b) A typical electron diffraction (ED) pattern of gold nanoparticles synthesized electrochemically is shown as the inset (lower right). (c) Elemental analysis of a single gold nanoparticle by EDS.

be noted that the gold particles were not pretreated or modified before TEM measurements.

The crystal structures of PVP-protected gold nanoparticles were investigated by high-resolution transmission electron microscopy (HRTEM) and electron diffraction pattern (ED). The HRTEM image of an individual particle (Figure 7a) reveals the resolved 2D lattice of gold. No obvious lattice defects were seen from this image of about 25×25 nm^2. The lattice spacing of 0.229 and 0.219 nm measured from different sites corresponds well to the (111) plane spacing for the face-centered cubic (fcc) gold (about 0.236 nm) within the experimental errors.[29,30] Figure 7b shows a typical ED pattern for fcc single crystals. The quite regular diffraction spot arrays further confirmed that an individual gold nanocrystal was a good single crystal rather than a twinned or multiply twinned nanocrystal. It is inferred that the PVP-protected gold nanocrystals were the fcc-structured polyhedral nanocrystals bounded by the relatively large {111} facets, whose morphology is probably similar to the gold single-crystalline bead prepared by melting one end of a pure gold wire in the hydrogen flame.[31] EDS analysis on the as-synthesized gold particles gave strong gold signals (Figure 7c), proving that individual particles in the close-packed aggregates were gold particles.

3.3. Particle Formation Mechanism. The formation mechanism of the PVP-protected gold nanocrystals is described as follows: (i) PVP and $AuCl_4^-$ anions form the multinuclear Au^{III}−PVP complexes through coordination of N and O atoms to Au^{III} ions, which involves the removal of partial Cl^- ions from $AuCl_4^-$ anions. PVP has been proved to be a good polymeric ligand system that coordinates easily to Ag^+,[32] Cu(II),[33] and Pt(IV)[19b] ions; moreover, the metal ions may be anchored to the PVP polymer through the coordination bonds between N, O atoms in PVP, and metal ions. (ii) On the basis of the electrochemical formation mechanism of metallic particles proposed, respectively, by Reetz and Helbig,[8a] Natter and Hempelmann,[8d] and Redriguez-Sanchez et al.,[16a] the electrochemical reduction of the Au^{III}−PVP complexes at the cathode/electrolyte interface is expected to generate Au^0 adatoms, followed by the formation of gold nuclei stabilized by PVP. As the space of individual Au^0 atoms in the PVP chain is short, collision of the neighboring Au^0 atoms results in the gold clusters. The suspensive electrode will be formed in the vicinity of the cathode when the electrolytic solution near the cathode contains a sufficient amount of the gold clusters.[34] The suspended particles move in the solution near the cathode, hit the cathode, accept its potential, and travel back to the solution. Because these charged gold particles can act as part of the cathode, other Au^{III} ions will get electrons not only from the cathode surface but also from these charged clusters,[6,34] leading to the formation of more gold nuclei. (iii) The electroreduction of the Au^{III}−PVP complexes and the growth of the gold nuclei proceed at the same time to form the gold nanoparticles, which is accompanied by the complete elimination of Cl^- ions. To produce the final fcc-structured nanocrystals, the gold nuclei probably grow through electrochemical reduction of the remnant Au^{III} ions on the lowest-energy {111} planes of gold nuclei to form the stable nanoparticles with atomic shell structures such as 2-shell (55 atoms), 3-shell (147 atoms), and 4-shell (309 atoms) nanoparticles.[19b] The absence of the octahedral or tetrahedral nanocrystals in Figure 5a implied that the selective interaction between PVP and various crystallographic planes of fcc gold could decrease the growth rate along the ⟨111⟩ direction or increase the growth rate along the ⟨100⟩ direction.[35] (iv) The gold nanoparticles are stabilized by coordination of partial surface gold atoms to the N and O atoms of PVP. Part of the main chain of PVP is expected to be adsorbed on the surface gold atoms by hydrophobic interaction.[19b] The PVP is able to protect the growing gold clusters from coalescence. The steric effect arising from the long polyvinyl chain of PVP on the surface of gold particles can contribute to antiagglomeration, whereas the chemical bond between the PVP and gold particles may prohibit aggregation of the formed gold particles.

In this way, the size- and/or shape-controlled synthesis of gold nanocrystals is possible by a simple electrochemical process under the condition where the sufficient quantity of PVP is employed as the stabilizer for the gold clusters. Moreover, the good homogeneity of gold nanocrystals in size and shape is very advantageous to their spontaneous self-assembly into compact 2D arrays, as shown in Figure 6a.

3.4. 1D Self-Assembly. The electroreduction of Au^{III}−PVP complexes will generate many gold nuclei along the polyvinyl chain of PVP, which subsequently grow into the nanocrystals. Seeing that a PVP macromolecule most likely adopts a pseudo-random coil conformation, the use of PVP offers a great probability to make multiform 1D nanoparticle aggregates. For example, using PVP as the templates to direct one-dimensional growth or self-assembly of silver nanoparticles, Giersig and co-workers[28] prepared fcc single-crystalline nanowires through aggregation of precursor silver nanoparticles, Deng et al.[36] synthesized the chainlike silver nanocrystals, and we organized silver particles photochemically synthesized into rodlike, wirelike, and chainlike nanostructures.[20] Additional attractable novel 1D nanostructures are presented in this paper. Figure 8a shows that numbers of gold nanocrystals made up a group of wonderful nanorings. The biggest nanoring (A) among them was a discontinuous ring of about 4.5 μm in length. The nanoparticle aggregates with analogous configuration were also seen in great abundance. Figure 8b exhibits some rod-shaped and arc-shaped nanoparticle aggregates, including a line-type nanorod (B) of 0.29 μm in length and 20.5 nm in average width and three long arc-shaped nanorods. These nanorings differ greatly from the submicrometer rings of particles indicated by Ohara and co-workers[37] in appearance and formation mechanism. The pearl-chainlike structural characteristic of the 1D nanostructures in Figure 8 indicates that these nanoaggregates formed not through the point-initiated uniaxial growth of the gold nuclei but rather by the self-assembly of nanoparticles along the PVP chains.[20,38] The aggregation of the precursor nanoparticles is thermodynamically favorable due to the decrease in overall surface. The driving force for the spontaneous self-organization of gold nanoparticles into the pearl-chainlike nanostructures should be the formation of dipolar moments within the nanoparticles.[38] It is possible that the attachment of particles occurring between the suitable crystallographic facets involves the fusion.[28] Although studies about self-assembly of colloidal particles are frequently reported, such interesting gold nanorings constructed by individual gold nanocrystals in a sample self-assembling manner are very rare. The unique structural property of these 1D gold nanoaggregates makes them applicable in electronics, catalysis, nanodevices, and other areas.

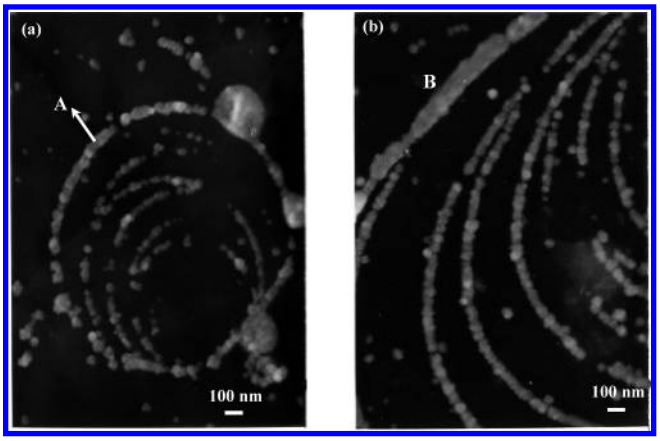

Figure 8. (a) TEM micrograph for a group of nanorings formed by self-assembly of individual gold nano crystals. (b) TEM micrograph for another set of rod-shaped and arc-shaped gold nanoparticle aggregates obtained from the same TEM sample.

3.5. Influence of PVP Concentration and Chain Length. Figure 9a shows the change of the absorbance with the PVPK90 concentration for typical electrochemical synthetic experiments carried out at an applied current of 100 mA and at a rotation rate of 1000 rpm. In the case of relatively low PVP concentration (10 g dm^{-3}), a wide absorption band was observed with a maximum centered at 546 nm in curve A, which is the characteristic surface plasmon excitation of spherical gold nanoparticles. Upon increasing the PVP concentration from 10 to 30 g dm^{-3}, the absorption band became more symmetrical, and a blue-shift appeared in the maximum of the plasmon peak, as indicated by curves B and C. The dependence of the characteristic absorbance band on the PVP concentration shows

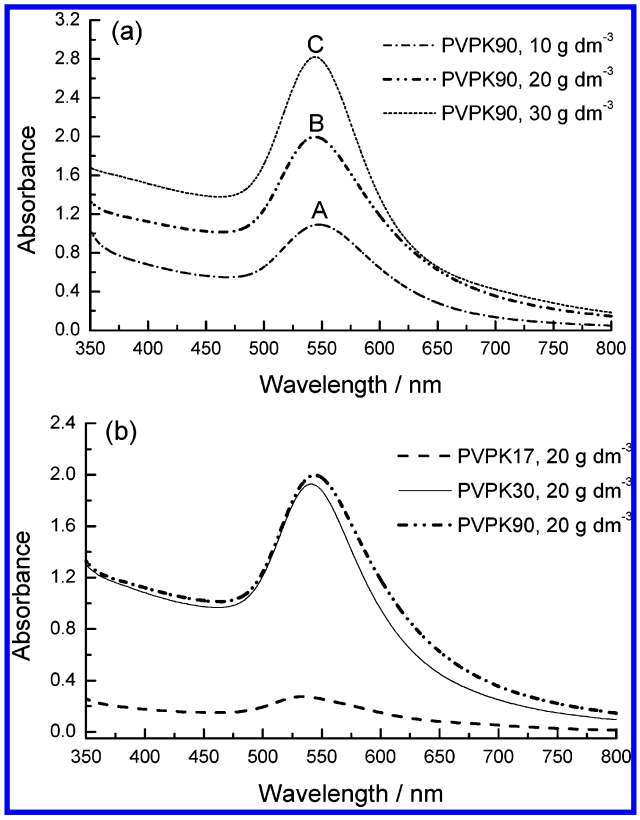

Figure 9. Influence of PVP concentration (a) and chain length (b) on the characteristic absorbance band of spherical gold nanoparticles synthesized electrochemically.

that the PVP protection effect against particle aggregation improves with the increase of PVP concentration. The relatively high PVP concentration is favorable for the electrochemical synthesis of gold nanoparticles with a small size and uniform size distribution. However, too high PVP concentration will make the electrolyte more viscous and therefore more difficult to handle in the electrochemical synthesis process. Our results have shown that the ideal molar ratio between PVP monomer and Au^{III} ions suitable for electrochemical synthesis of uniform gold nanoparticles ranges from 50:1 to 500:1.

Influence of the PVP chain length on the particle size was also investigated by using UV−vis spectroscopic study. As shown by Figure 9b, the UV−vis absorption spectra obtained using either PVPK90 or PVPK30 as the stabilizer displayed well-defined, symmetrical absorbance peaks, whereas the one obtained by using PVPK17 just showed a broad, nonsymmetrical plasmon band. It is believed that PVP with a short polyvinyl chain is disadvantageous to the electrochemical synthesis of gold nanoparticles with narrow particle size distribution.

Figure 10 shows TEM images for gold nanocrystals electrochemically synthesized by using PVPK17 and PVPK30 as the stabilizers. It can be seen that the chain length of PVP significantly affects the size and morphology of gold nanoparticles. The gold nanocrystals synthesized under protection of PVPK30 or PVPK17 were not as good in uniformity and in shape control as the PVPK90-protected gold nanocrystals. In addition, no regular 1D or 2D nanoaggregates were found in Figure 10, parts a and b. However, it is worth noticing that the gold nanocrystals of various shapes, such as triangular, hexagonal, and polyhedral crystallites, can be obtained at the same time when using PVPK17 as the stabilizer for gold nanocrystals. PVPK17 is expected to play an important role in synthesis of gold nanocrystals with special shape.

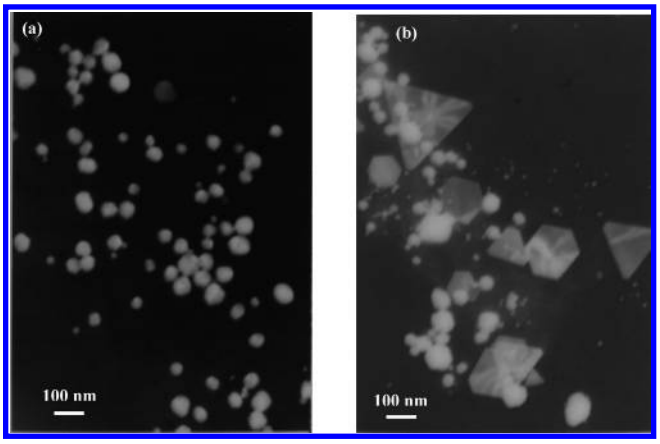

Figure 10. TEM images for gold nanocrystals electrochemically synthesized under protection of PVPK30 (a) or PVPK17 (b). Electrolytes are the aqueous solutions of 5.0×10^{-4} mol dm^{-3} $HAuCl_4$ + 0.1 mol dm^{-3} KNO_3 + 30 g dm^{-3} PVP.

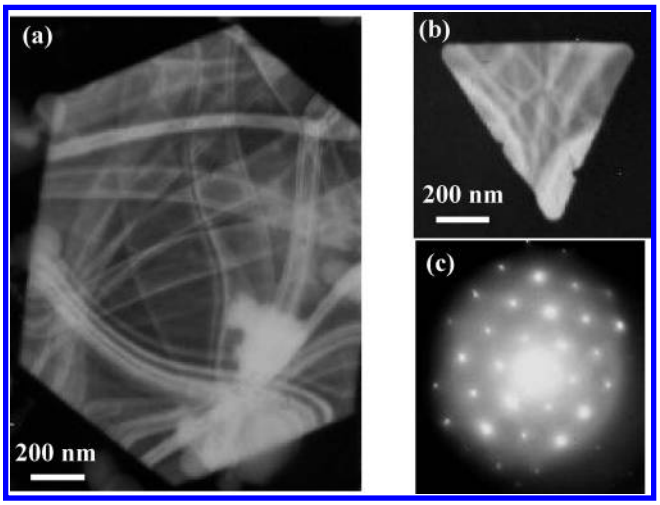

Figure 11. TEM images for a hexagonal (a) and a triangular (b) fragment scraped from the ultrathin film at the bottom of a glass bottle. The gold nanocrystals spontaneously self-assembled into an ultrathin single-crystalline film when the PVPK17-protected colloidal gold solution was placed in a small glass bottle for more than 3 days. (c) Electron diffraction (ED) pattern of the hexagonal fragment.

3.6. Formation of a Single-Crystalline Film. The PVP chain length also has a great influence on the stability of the gold nanocrystals. The gold nanocrystals synthesized under protection of PVPK30 or PVPK90 were very stable and could remain unchanged for several months, without the occurrence of any precipitate. In contrast, the gold nanocrystals protected by PVPK17 ($\bar{M}_w \approx 10000$) had a relatively low stability. When such a gold colloid was placed in a small glass bottle for more than 3 days, a thin pink film was found to gradually form on the wall and at the bottom. The film was scraped, and some fragments were carefully collected. Figure 11, parts a and b, shows beautiful TEM images for a hexagonal fragment (≈1.7 μm^2) and a triangular fragment, respectively. The existence of many Kikuchi lines provides powerful evidence that the fragment was a perfect crystal. The hexagonal symmetry of an electron diffraction pattern (Figure 11c) further proved that the hexagonal fragment was a single crystal bounded by large {111} facets. Obviously, the thin film is not a common film but an ultrathin single-crystalline film. We believe that the formation of the ultrathin film is closely related to the important role of the PVP polymer although the exact formation mechanism remains unknown. Due to insufficient protection of PVPK17, many small particles recrystallized and gradually fused into a

large crystal.[38] Moreover, the growth rate of gold nuclei along the ⟨111⟩ direction was greatly limited, thereby forming a single-crystal film bounded by large {111} facets.

4. Conclusion

Gold nanocrystals with controllable size were synthesized through a simple electroreduction using PVP as the stabilizer for gold nanocrystals. The uniformity of gold nanocrystals in size and shape is one of the conditions necessary for the self-assembly of the nanocrystals into the ordered 2D close-packed arrays. The aggregation of PVPK17-protected gold nanocrystals resulted in the formation of an ultrathin single-crystalline film. PVP not only plays an important role in the particle size (or shape) control, preventing the gold clusters from coalescing, reducing or enhancing the growth rate of certain crystal planes, but also can induce individual gold nanocrystals to constitute regular 1D nanostructures. The nanoparticle self-assembling technique based on PVP provides a good path to organize nanoparticles into various 1D and 2D nanostructured materials.

Acknowledgment. This work was supported by the Scientific Research Award Fund for Excellent Middle-Aged and Young Scientists of Shandong Province (02BS053) and the Visiting Scholar Foundation of Key Laboratory in Shandong University and National Natural Science Foundation of China (20573068).

References and Notes

(1) Jana, N. R.; Peng, X. *J. Am. Chem. Soc.* **2003**, *125*, 14280.
(2) Wu, Y.; Yang, P. *J. Am. Chem. Soc.* **2001**, *123*, 3165.
(3) Elghanian, R.; Storhoff, J. J.; Mucic, R. C.; Letsinger, R. L.; Mirkin, C. A. *Science* **1997**, *277*, 1078.
(4) Collier, C. P.; Saykally, R. J.; Shiang, J. J.; Henrichs, S. E.; Heath, J. R. *Science* **1997**, *277*, 1978.
(5) (a) Sun, Y.; Xia, Y. *Science* **2002**, *298*, 2176. (b) Sun, Y.; Mayers, B.; Xia, Y. *Nano Lett.* **2003**, *3*, 675.
(6) Yin, B. S.; Ma, H. Y.; Wang, S. Y.; Chen, S. H. *J. Phys. Chem. B* **2003**, *107*, 8898.
(7) Bradley, J. S. In *Clusters and Colloids*; Schmid, G., Ed.; VCH: Weinheim, **1994**; Chapter 6.
(8) (a) Reetz, M. T.; Helbig, W. *J. Am. Chem. Soc.* **1994**, *116*, 7401. (b) Reetz, M. T.; Winter, M.; Breinbauer, R.; Thurn-Albrecht, T.; Vogel, W. *Chem.*—Eur. J. **2001**, *7*, 1084. (c) Reetz, M. T.; Helbig, W.; Quaiser, S. A.; Stimming, U.; Breuer, N.; Vogel, R. *Science* **1995**, *267*, 367. (d) Natter, H.; Hempelmann, R. *Electrochim. Acta* **2003**, *49*, 51.
(9) Jana, N. R. *Angew. Chem., Int. Ed.* **2004**, *43*, 1536.
(10) Korgel, B. A.; Fitzmaurice, D. *Adv. Mater.* **1998**, *10*, 661.
(11) Zhu, J.; Liu, S.; Palchik, O.; Koltypin, Y.; Gedanken, A. *Langmuir* **2000**, *16*, 6396.
(12) Pacholski, C.; Kornowski, A.; Weller, H. *Angew. Chem., Int. Ed.* **2002**, *41*, 1188.
(13) (a) Wu, C. G.; Bein, T. *Science* **1994**, *264*, 1757. (b) Brumlik, C. J.; Martin, C. R. *J. Am. Chem. Soc.* **1991**, *113*, 3174. (c) Parthasarathy, R.; Martin, C. R. *Nature* **1994**, *369*, 298. (d) Zhang, Z.; Gekhtman, D.; Dresselhaus, M. S.; Ying, J. Y. *Chem. Mater.* **1999**, *11*, 1659. (e) Martin, C. R. *Science* **1994**, *266*, 1961.
(14) (a) Zach, M. P.; Kwokh, N.; Penner, R. M. *Science* **2002**, *290*, 2120. (b) Zach, M. P.; Penner, R. M. *Adv. Mater.* **2000**, *12*, 878.
(15) Sun, Y.; Xia, Y. *Adv. Mater.* **2002**, *14*, 833.
(16) (a) Rodriguez-Sanchez, L.; Blanco, M. C.; Lopez-Quintela, M. A. *J. Phys. Chem. B* **2000**, *104*, 9683. (b) Rodriguez-Sanchez, M. L.; Rodrigues, M. J.; Blanco, M. C.; Rivas, J.; Lopez-Quintela, M. A. *J. Phys. Chem. B* **2005**, *109*, 1183.
(17) (a) Mohamed, M. B.; Ismail, K. Z.; Link, S.; El-Sayed, M. A. *J. Phys. Chem. B* **1998**, *102*, 9370. (b) Yu, Y.-Y.; Chang, S. S.; Lee, C.-L.; Wang, C. R. C. *J. Phys. Chem. B* **1997**, *101*, 6661. (c) Chang, S. S.; Shih, C.-W.; Chen, C.-D.; Lai, W.-C.; Wang, C. R. C. *Langmuir* **1999**, *15*, 701.
(18) (a) Pastoriza-Santos, I.; Liz-Marzan, L. M. *Langmuir* **2002**, *18*, 2888. (b) Pastoriza-Santos, I.; Liz-Marzan, L. M. *Nano Lett.* **2002**, *2*, 903.
(19) (a) Teranishi, T.; Hosoe, M.; Tanaka, T.; Miyake, M. *J. Phys. Chem. B* **1999**, *103*, 3818. (b) Teranishi, T.; Miyake, M. *Chem. Mater.* **1998**, *10*, 594.
(20) Ma, H. Y.; Jiao, Y. L.; Yin, B. S.; Wang, S. Y.; Zhao, S. Y.; Huang, S. X.; Pan, W.; Chen, S. H.; Meng, F. J. *ChemPhysChem* **2004**, *5*, 713.
(21) Ma, H. Y.; Yin, B. S.; Wang, S. Y.; Jiao, Y. L.; Pan, W.; Huang, S. X.; Chen, S. H.; Meng, F. J. *ChemPhysChem* **2004**, *5*, 68.
(22) (a) Sun, Y.; Gates, B.; Mayers, B.; Xia, Y. *Nano Lett.* **2002**, *2*, 165. (b) Sun, Y.; Yin, Y.; Mayers, B. T.; Herricks, T.; Xia, Y. *Chem. Mater.* **2002**, *14*, 4736.
(23) (a) Garotenuto, G.; Pepe, G. P.; Nicolais, L. *Eur. Phys. J. B* **2000**, *16*, 11. (b) Garotenuto, G. *Appl. Organomet. Chem.* **2001**, *15*, 344.
(24) Hamelin, A. *J. Electroanal. Chem.* **1996**, *407*, 1
(25) Dean, J. A. In *Lange's Handbook of Chemistry*, 15th ed.; McGraw-Hill: Singapore, 1999; p 8.128.
(26) Dean, J. A. In *Lange's Handbook of Chemistry*, 15th ed.; McGraw-Hill: Singapore, 1999; p 8.140.
(27) (a) Taleb, A.; Petit, C.; Pileni, M. P. *J. Phys. Chem. B* **1998**, *102*, 2214. (b) Petit, C.; Lixon, P.; Pileni, M. P. *J. Phys. Chem.* **1993**, *97*, 12974.
(28) Giersig, M.; Pastoriza-Santos, I.; Liz-Marzan, L. M. *J. Mater. Chem.* **2004**, *14*, 607.
(29) Zhang, D.; Qi, L.; Ma, J.; Cheng, H. *Chem. Mater.* **2001**, *13*, 2753.
(30) Li, X.; Li, Y.; Tan, Y.; Yang, C.; Li, Y. *J. Phys. Chem. B* **2004**, *108*, 5192.
(31) Itaya, K. *Prog. Surf. Sci.* **1998**, *58*, 121.
(32) Zhang, Z.; Zhao, B.; Hu, L. *Solid State Chem.* **1996**, *121*, 105.
(33) Hu, J. C.; Cao, Y.; Yang, P.; Deng, J. F.; Fan, *J. Mol. Catal. A* **2002**, *185*, 1.
(34) Socol, Y.; Abramson, O.; Gedanken, A.; Meshorer, Y.; Berenstein, L.; Zaban, A. *Langmuir* **2002**, *18*, 4736.
(35) Wang, Z. L. *J. Phys. Chem. B* **2000**, *104*, 1153.
(36) Deng, Y.; Wei, G.; Nan, C. *Chem. Phys. Lett.* **2003**, *368*, 639.
(37) Ohara, P. C.; Heath, J. R.; Gelbart, W. M. *Angew. Chem., Int. Ed. Engl.* **1997**, *36*, 1078.
(38) Tang, Z.; Kotov, N. A.; Giersig, M. *Science* **2002**, *297*, 237.